 http://dx.doi.org/10.14500/aro.12258

High Reflectivity Compounds of Cadmium Sulfide/Magnesium Fluoride Distribution Bragg Reflectors: Design, Simulation, and Comparative Analysis

Jihad A. Swara, Faten A. Ismael Chaqmaqchee and Khalid N. Sediq†

Department of Physics, Faculty of Science and Health, Koya University,
Koya 44023, Kurdistan Region – F.R. Iraq

***Abstract*—This work investigates the optical performance of a distributed Bragg reflectors (DBRs) structure, designed with a Matlab program using inorganic compounds of cadmium sulfide (CdS) and magnesium fluoride (MgF_2) with a central operational wavelength of 650 nm. Because CdS (high index) and MgF_2 (low index) have very different refractive indices, the proposed DBR can reflect light effectively using fewer alternating layers. The Transfer Matrix Method simulation method indicates that the DBR structure reaches its maximum reflectivity with just six-layer pairs, emphasizing its optical efficiency and structural simplicity. A comparative analysis with other DBR structures demonstrates the superior performance of CdS/MgF_2 DBR, which exhibits a broader usable stopband at around 181.82 nm, the highest bandwidth of 298.49 nm, and a relatively moderate Q-factor (2.18), indicative of an enhanced reflector response. These results establish CdS/MgF_2 DBR as highly efficient reflectors that are well-suited for optical systems functioning in the visible spectrum.**

***Index Terms*—Compounds of cadmium sulfide/magnesium fluoride, Distribution Bragg reflector, Full width at half maximum, Q-factor, Reflectance, Stopband.**

I. Introduction

A distributed Bragg reflector (DBR) is a crucial part of contemporary optical technology, based on interference from thin films. DBRs consist of many stacked pairs of alternating dielectrics. Each pair comprises two materials with varying refractive indices (Assafli, et al., 2016). There are three types of DBRs: air-gap-based, dielectric, and epitaxial (Kumar, et al., 2019). The thickness of the multilayered structure of the DBR that consists of high-low refractive index contrast can be set to λ/4. The constructive interference occurs at the Bragg wavelength λ, causing the structure to operate as a mirror with a tunable reflective surface and variable spectral bandwidth (Coldren, et al., 2012).

Recent research has continued to explore and optimize DBRs for a wide range of photonic and optoelectronic applications across visible and near infrared regions. Inorganic materials remain a focal point due to their thermal stability, high refractive index contrast, and compatibility with existing fabrication technologies. For instance, materials such as titanium dioxide (TiO_2)/silicon dioxide (SiO_2) (Gao, et al., 2020) (Miao, et al., 2023), ZnS/CaF_2 (Muallem, et al., 2015), HfO_2/SiO_2 (Cui, et al., 2022), and SiN_x/SiO_y (Rodríguez Lamoso and Preu, 2025) pairs have been widely used in recent DBR structures to enhance reflectivity, stopband width, and center wavelength, which are essential parameters for optical filtering. However, these materials have been shown promising results; the exploration of alternative material systems remains important for expanding, reducing cost, or achieving specific optical responses. The suitability of compounds of cadmium sulfide (CdS)/magnesium fluoride (MgF_2) as promising DBR pairs presents an offering a compelling choice due to strong refractive index contrast, potential for wide stopbands with fewer layers, and excellent performance within the visible spectral range. These inorganic multilayer systems have found use in light-emitting diodes (LEDs), vertical cavity surface emitting lasers (VCSELs), optical filters, sensors, and photodetectors, where precise control of reflectance and bandwidth is crucial (Zhang, et al., 2019; Dai, et al., 2016; Valligatla, et al., 2012; Ma, et al., 2006); (Haglund, et al., 2016).

DBR can be designed to reflect the light of ultraviolet (Alias, et al., 2018), visible, and infrared regions (Chaqmaqchee, 2022; Sediq, Muhammadsharif, and Muhammad, 2022). The reflectivity spectrum for the perpendicular and parallel polarization directions of light is calculated using the transfer matrix method (TMM) (Palo and Daskalakis, 2023).

The TMM is a well-established widely and flexible computational approach for analyzing the propagation of electromagnetic waves through stratified optical media. It is

ARO-The Scientific Journal of Koya University
Vol. XIII, No. 2 (2025), Article ID: ARO.12258. 7 pages
DOI: 10.14500/aro.12258
Received: 07 May 2025; Accepted: 09 August 2025
Regular research paper; Published: 05 September 2025
†Corresponding author's e-mail: khalid.sediq@koyauniversity.org

especially effective for multilayer thin-film structures, such as DBRs, as it enables precise calculation of reflectance, transmittance, and internal electric field distributions by accounting for the refractive indices and thicknesses of individual materials (Yeh and Hendry, 1990). Fresnel's and Maxwell's equations based on the TMM method were used for dielectric media to define boundary conditions at the interfaces of multilayer structures. The computed reflectivity is influenced by the refractive index contrast between the two materials and the absorption losses in the mirrors (Mohammed, 2019; Byrnes, 2016). Thus, the TMM is typically employed to evaluate the reflectance, transmittance, and absorptance of the DBR layers at an interface.

In this study, DBR structure-based CdS/MgF_2 is designed using the MATLAB program, which is limited to normal incidence and does not account for variations in polarization or incidence angle. These inorganic compounds (Inorganic materials are widely used in DBRs due to their favorable optical properties including high transparency and compatibility with high index contrast designs) are utilized as a chemically stable, cost-effective, and easily fabricated material system. Its superior spectral reflectivity compared to other DBR structures which makes its potential as a strong candidate for integrated optical communication systems and broadband optical filter design.

II. Materials and Methods

A. Materials Selection

Illustrated in Fig. 1, the refractive indices of CdS and MgF_2 in the visible to infrared range are approximately n_{Cds} = 2.4637 (Bieniewski and Czyzak, 1963) and n_{MgF2} = 1.3767 (Dodge, 1984), respectively, demonstrating the significant optical contrast between the two materials.

For the several reasons, choosing both materials (CdS/MgF_2) to produce DBR at 650 nm. First, CdS/MgF_2 exhibits low absorptance and high transparency in the visible range, particularly around 650 nm (Polyanskiy, 2024). Second,

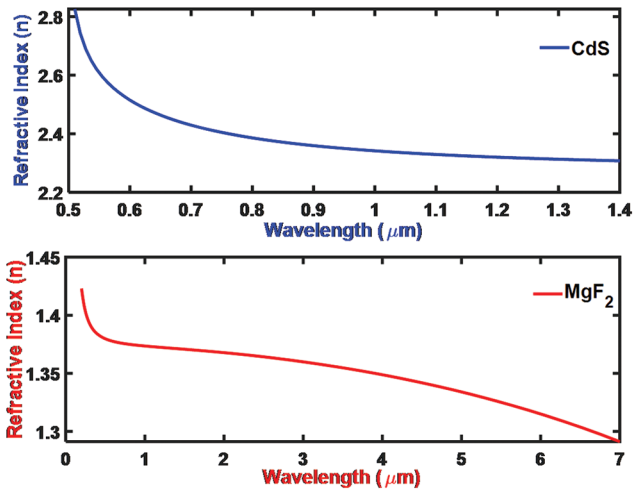

Fig. 1. Refractive index versus wavelength for compounds of cadmium sulfide and magnesium fluoride.

light at 650 nm corresponds to the red region of the visible spectrum, which is widely utilized in various optoelectronics applications. These include laser diodes, commonly used in laser pointers and optical storage (Jambunathan and Singh, 2002), optical filters such as bandpass and stopband filters (Dai, et al., 2016), red LEDs (Shaaban, et al., 2022), sensors including reflectometric sensors and fluorescence-based sensors (Palo and Daskalakis, 2023), photodetectors, red enhanced photodetectors (Butt, et al., 2016), and VCSELs used in barcode scanners, optimal mice, and consumer electronics (Zhang, et al., 2019). Third, both materials have a high refractive index contrast; this strong contrast is a main reason for achieving high reflectivity with fewer pairs. Fourth, both CdS and MgF_2 are inorganic materials that are chemically stable and compatible with conventional thin film deposition techniques, which simplify the fabrication process. Finally, CdS has a relatively high refractive index, that is used as the first layer in the DBR stack. The positioning enhances the reflectance at the air/DBR interface, as a greater refractive index contrast between the medium of air and the first layer leads to stronger reflection.

B. Optical Design Consideration

To design a DBR structure, some parameter affects the central wavelength to be reflected, so they affect the number of pairs and the way it is placed. The thickness of each layer determines the central wavelength to be reflected. The thickness of each layer at 650 nm is calculated by:

$$t_H = \frac{\lambda_0}{4n_H} \quad (1)$$

$$t_L = \frac{\lambda_0}{4n_L} \quad (2)$$

where t_H and t_L correspond to the high- and low-index layer thickness, with n_H and n_L denote the refractive index of high- and low-index materials, respectively, while λ_0 denotes the center wavelength (Sediq, et al., 2023; Jambunathan and Singh, 1997). The calculated thicknesses were t_H = 65.958 mm and t_L = 118.036 mm. SiO_2 was employed as the substrate material for the device.

The design structure of the DBR is illustrated in Fig. 2. The first layer of CdS has a high refractive index material, followed by a MgF_2 layer of low refractive index material. Usually, these materials were selected for two reasons. First, when light moves from a medium where it slows down of higher refractive index to one where it speeds up of lower refractive index, partial reflection occurs with a π phase shift, which is essential for constructive interference in the DBR stack (Chaqmaqchee, 2012). Upon high-to-low interfaces, a 180° phase shift is important because it results in the constructive accumulation of reflections from several layers (Sale, 1995). If the layer arrangement is reversed, a disturbance in the interference pattern may occur, resulting in reduced overall reflectivity. Second, starting with a high index material creates a stronger refractive index contrast with air, enhancing the initial reflectivity at the air DBR

http://dx.doi.org/10.14500/aro.12258

interface, and therefore increasing the reflectivity of the DBR structure (Sediq, et al., 2023; Sharhan, 2020).

III. Results and Discussion

A. Reflectance and Refractive Index

The reflectivity of DBR is directly influenced by both the layer periods and the refractive index between different materials. This relationship can be expressed as follows (Yeh and Hendry, 1990):

$$R = \left[\frac{1 - \left(\frac{n_L}{n_H} \right)^{2m}}{1 + \left(\frac{n_L}{n_H} \right)^{2m}} \right]^2 \quad (3)$$

where m refers to the total number of alternating layer periods in DBR. This reflectivity calculation is ideal and lossless materials in the simulation that does not include intrinsic absorption losses or scattering losses or other potential loss mechanisms into the MATLAB model.

Based on equation (3), the peak of reflectivity as a function of the number of DBR pairs (m) was calculated and plotted for various materials of CdS/MgF_2, HfO_2/SiO_2, GaAs/AlAs, GaN/AlN, and InP/InGaAsP, as shown in Fig. 3. In which their refractive indices at 650 nm were (2.4637, 1.3767), (1.8931, 1.4565) (Al-Kuhaili, 2004; Malitson, 1965), (3.8300, 3.0944) (Aspnes, et al., 1986; Fern and Onton, 1971), (2.3803, 2.1481) (Barker Jr and Ilegems, 1973; Pastrňák and Roskovcová, 1966), and (3.5195, 3.3970) (Aspnes and Studna, 1983; Adachi, 1989), respectively.

It was observed that 6 pairs of CdS/MgF_2 were required to reach 100% of reflectance. On the other hand, systems such as GaAs/AlAs reach only 70% of reflectance at the same pair numbers. Therefore, it is evident that just a few pairs are needed to get a certain reflectivity when the index contrast ratio is large (Chaqmaqchee, 2016). Fig. 3 shows the reflectance pattern versus wavelength for various DBR systems working at the same central wavelength.

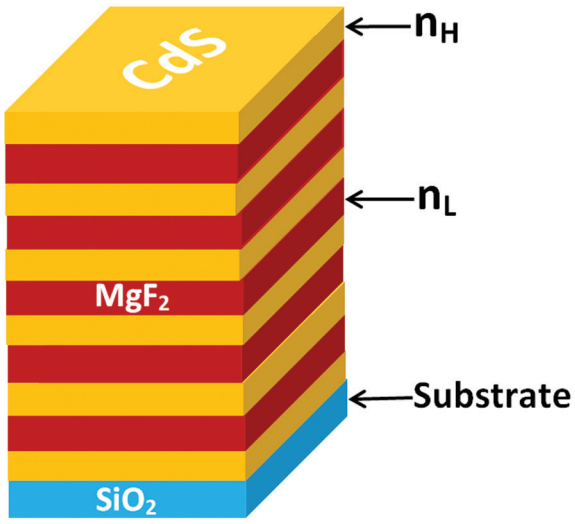

Fig. 2. Design and structure of a distributed Bragg reflector with a stacked pair of compounds of cadmium sulfide/magnesium fluoride onto a silicon dioxide substrate.

B. Reflectance and Number of Pairs

By using equation 4, the reflectivity for DBRs using different layer pairs ranging from 2 to 10 layers was calculated and plotted as presented in Fig. 4. Each curve illustrates the reflectance versus wavelength (in nm).

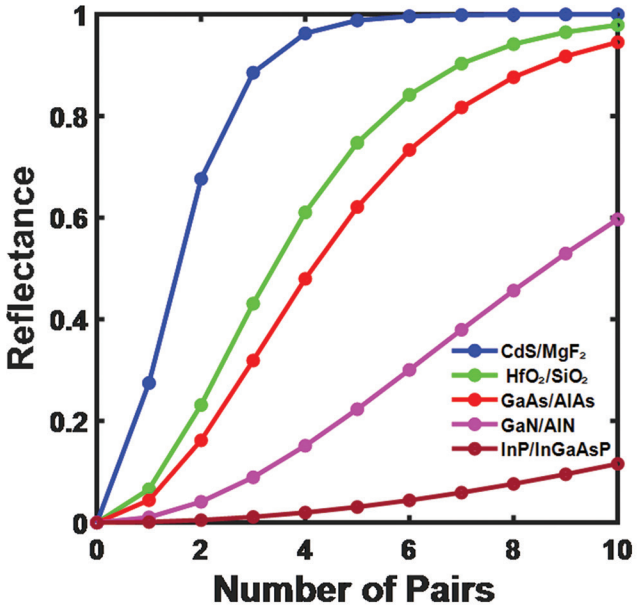

Fig. 3. Reflectance value versus number of pairs for 5 different distributed Bragg reflector systems.

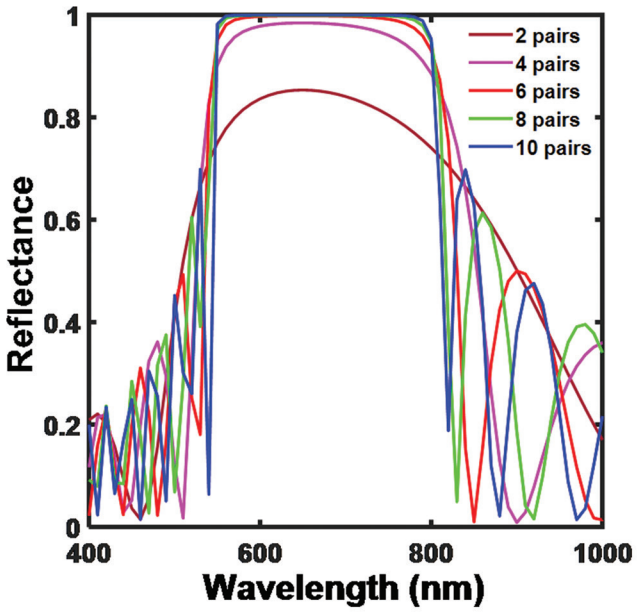

Fig. 4. Reflectance spectrum versus number of pairs from 2 to 10 pairs for compounds of cadmium sulfide/magnesium fluoride.

$$R = \left[\frac{\mu_0 B - C}{\mu_0 B + C}\right]^2 \quad (4)$$

where B, C, and μ_0 are the electric field, the magnetic field amplitudes at the boundary, and the optical admittance of the emission layer, respectively (Chaqmaqchee, Salh, and Sabri, 2020); (Shaaban, et al., 2022).

For two pairs of layers, the reflectance value is small and has a broad boundary. As the number of DBR layer pairs increases up to 10, it results in a corresponding rise in peak reflectance approaching unity (100%), and the edges of the peak become sharper.

A comparison graph was plotted to show the variation of reflectance spectra or Bragg reflectors for six pairs of different materials, as shown in Fig. 5. It shows the effect of different material combinations on reflectivity and the width of the peak spectrum. Therefore, an increase in refractive contrast between the two materials leads to a rise in both peak reflectance and spectral bandwidth. Among the studied material systems, CdS/MgF_2 exhibits the highest refractive index contrast and shows the greatest reflectance and the broadest reflectance peak.

According to energy conservation law, the incident light wave on a medium is separated into three parts: Reflectance (R), transmittance (T), and absorptance (A) (Troitskiĭ, 2002). Determining the transmittance and absorptance of a DBR is useful for accurately designing and analyzing the optical behavior of photonic systems. Absorptance measurement helps to identify optical losses arising from intrinsic material absorption, structural defects, or non-ideal interfaces within the DBR. In contrast, transmittance analysis helps understand how effectively the DBR performs to reflect a specified wavelength. Transmittance and absorptance are essential optical parameters used to characterize the energy flow through a DBR structure, which are expressed as follows:

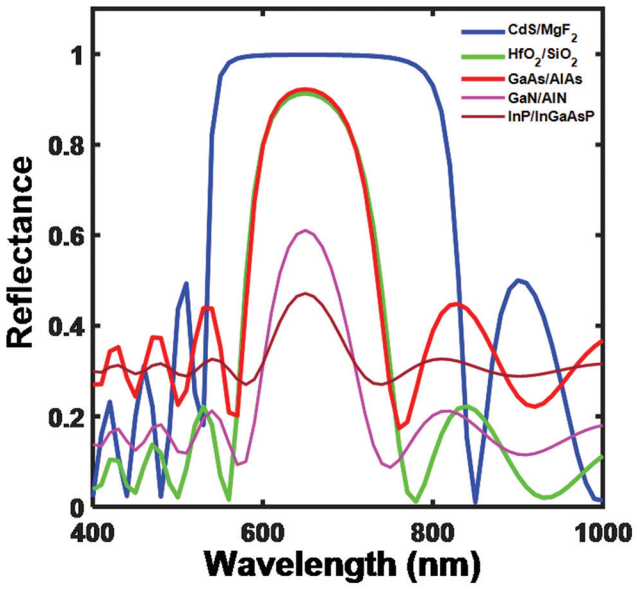

Fig. 5. Reflectance spectrum versus wavelength (nm) at 6 pairs for 5 different materials.

$$T = \frac{4\mu_0\mu_{sub}}{\left|\mu_0 B + C\right|^2} \quad (5)$$

$$A = 1 - R - T \quad (6)$$

where μ_0 is the optical admittance of the emission layer, μ_{sub} is the optical admittance of the substrate, and A is the absorptance (Chaqmaqchee, 2012); (Min, et al., 2022). Absorption was estimated theoretically based on the energy conservation law, rather than from actual absorption coefficients of the materials. In another words, absorption was not directly simulated using real simulation parameters.

According to equations (4), (5), and (6), the optical spectra of reflectance, transmittance, and absorptance versus wavelength for 6 pairs for CdS/MgF_2, as shown in Fig. 6. At a visible to near IR range (550 nm to 800 nm), spectra of transmittance and absorptance have a very low value (approximately equal to zero). This is due to the strong reflectivity of DBR in this range of wavelengths. The selected wavelength range encompasses the central operational wavelength is 650 nm, which is the design target of Bragg reflectors. This range allows us to analyze the reflectance behaviour not only at the central wavelength but also across a broad section of the visible spectrum, where both CdS and MgF_2 demonstrate favorable optical properties. In addition, since the study focuses on applications within the visible range, this spectral window is relevant for optical filter devices.

C. Stopband Width

The width of the stopband in the DBR helps to determine its ability to provide reflection across a particular band of wavelengths. The fractional stopband is influenced by the refractive indices of the high and low index materials, where

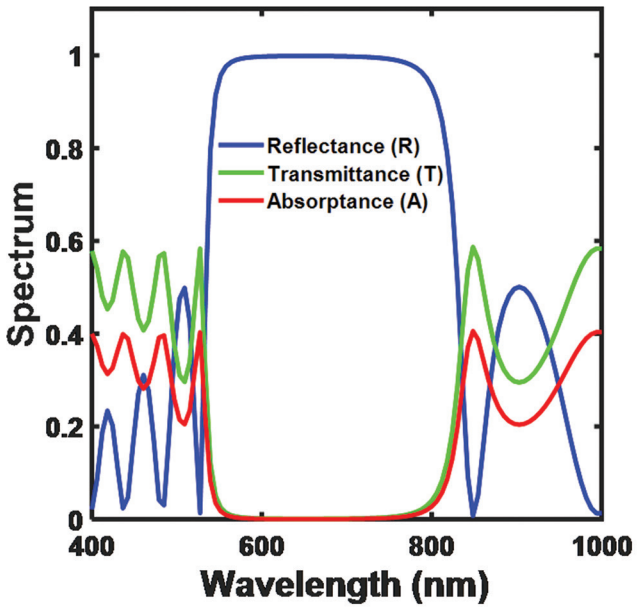

Fig. 6. Optical spectra of reflectance and transmittance and absorptance versus wavelength (nm) of 6 pairs for compounds of cadmium sulfide/ magnesium fluoride.

http://dx.doi.org/10.14500/aro.12258

the relationship is mathematically expressed as follows (Macleod and Macleod, 2010):

$$\Delta\lambda_{max} = \frac{4\lambda_B}{\pi}\sin^{-1}\left(\frac{\Delta n}{n_H + n_L}\right) \quad (7)$$

where $\Delta\lambda_{max}$ is the stopband width within the high reflectance band of the DBR mirrors, λ_B is the Bragg wavelength or central wavelength, and Δn is the refractive index difference of the two materials ($\Delta n = n_H - n_L$). In this context, $\Delta\lambda_{max}$ represents the stopband width of the high reflectance band in the DBR mirror, which is directly proportional to both the Bragg wavelength (λ_B) and refractive index contrast Δn (Zhang, et al., 2019). According to equation 7, $\Delta\lambda_{max}$ for CdS/MgF_2, HfO_2/SiO_2, GaAs/AlAs, GaN/AlN, and InP/InGaAsP were equal to 237.495 nm, 108.181 nm, 88.085 nm, 42.455 nm, and 14.658 nm, respectively. As a result, CdS/MgF_2 has the maximum stopband width value, in comparison with the other mentioned material systems (Palo and Daskalakis, 2023).

Equation (7) is a general formula for stopband width, and it does not include the number of pairs; therefore, an alternative stopband law was used that called usable stopband width ($\Delta\lambda_{usable}$). It is calculated when the reflectance is equal to or greater than 0.99 ($R \geq 99\%$), as illustrated in Fig. 7. Here, the horizontal dashed line represents the selected range of reflectance equal to or greater than 99%.

Fig. 8 illustrates the relationship between the usable stopband width and the number of pairs of materials (CdS/MgF_2, HfO_2/SiO_2, GaAs/AlAs, GaN/AlN, and InP/InGaAsP). All calculations show that the CdS/MgF_2 based DBR has a higher usable stopband width at around 181.82 nm using 6-pair layers and crosses its maximum usable stopband width much faster than others. To reach the plateau, the number of pairs should be equal to 14 pairs, depicting a very drastic rise in usable stopband width when a pair increases. It shows that the greater refractive index contrast between various materials leads to more effective stopband widening even with fewer layers, and it was proven that the number of pairs is effective and directly proportional to the usable stopband width until it reaches the maximum value or plateau; after this point, it does not affect the usable stopband width.

D. Full Width at Half Maximum (FWHM)

The FWHM of a DBR refers to the spectral width of the reflectance peak measured at half of its magnitude value. Their analysis allows the determination of DBR performance quality. The FWHM is calculated according to the following principles:

$$Half\ \ maximum\ (H_M) = \frac{R_{max} + R_{min}}{2} \quad (8)$$

$$FWHM = \lambda_l - \lambda_f \quad (9)$$

where R_{max} and R_{min} are the maximum and minimum points of the reflectance peak, respectively. λ_l and λ_f are the last and first points of the wavelength where reflectance equals the half-max level.

Based on equations (8) and (9), the FWHM versus the number of DBR pairs is calculated for CdS/MgF_2, HfO_2/SiO_2, GaAs/AlAs, GaN/AlN, and InP/InGaAsP structures. The FWHM for CdS/MgF_2 DBR using 6-pairs is around 300 nm. The FWHM decreases with an increasing number of pairs for all materials because the reflectance peak becomes sharper (Xu, et al., 2021), as illustrated in Fig. 9.

E. Quality Factor (Q-factor)

The Q-factor of a DBR is a fundamental metric used to quantify the sharpness of its reflectance stopband (Macleod and Macleod, 2010) and describes how narrow and well-

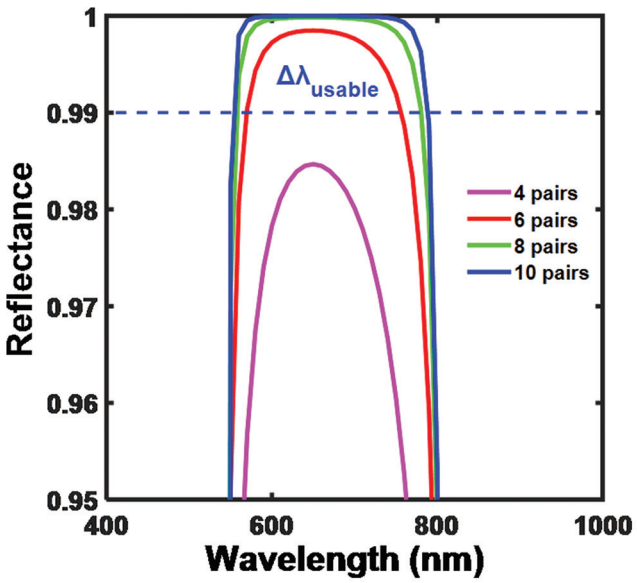

Fig. 7. Selection and representation $\Delta\lambda_{usable}$ of a ratio of reflectance with the wavelength (nm) for compounds of cadmium sulfide/magnesium fluoride.

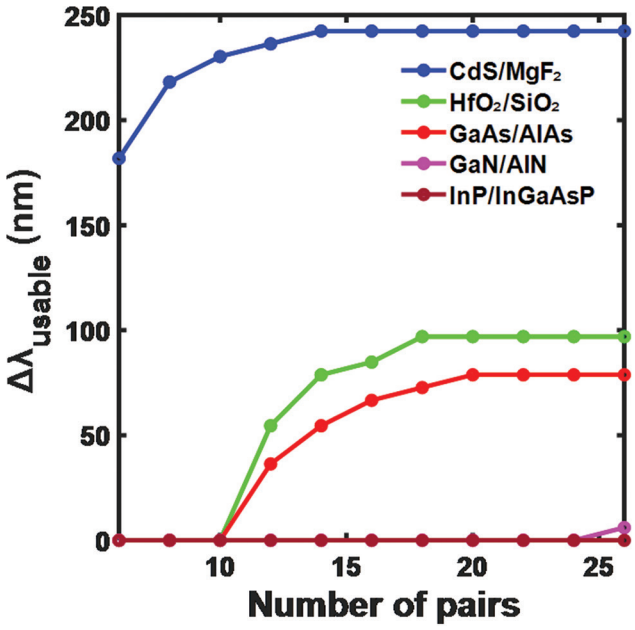

Fig. 8. Usable stopband width versus the number of pairs for five different materials.

defined the resonance is relative to its center frequency (Yariv, 1997). It is mathematically defined as:

$$Q = \frac{\lambda_0}{\Delta\lambda} \quad (10)$$

where λ_0 denotes the central wavelength and $\Delta\lambda$ represents the FWHM of the reflectance peak. The dependence of the Q-factor on the number of pairs in the CdS/MgF_2 DBR structure is illustrated in Fig. 10. The observed behavior is due to the inverse relationship between the Q-factor and the FWHW. The narrowing of the FWHM with an increase in pairs results in a corresponding rise in Q-factor. For example, the Q-factor in CdS/MgF_2 DBR is approximately 1.54 with 2 layers and 2.18 with 6-layer pairs, corresponding to a FWHM of 422.11 nm and 298.49 nm, respectively. As the number of pairs increases to 16 pairs, the Q-factor reaches 2.51 with a reduced FWHM of 259.30 nm. A lower Q-factor indicates a broader spectral bandwidth, not a narrower one (Kogelnik and Shank, 1972).

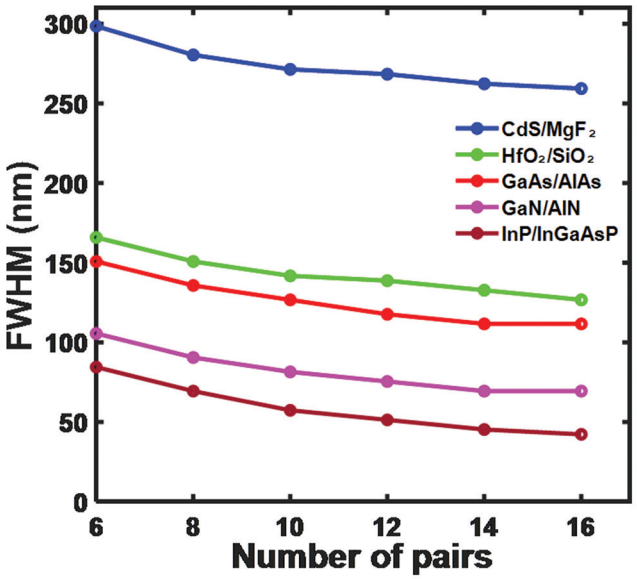

Fig. 9. Full width at half maximum versus number of pairs for five different inorganic materials.

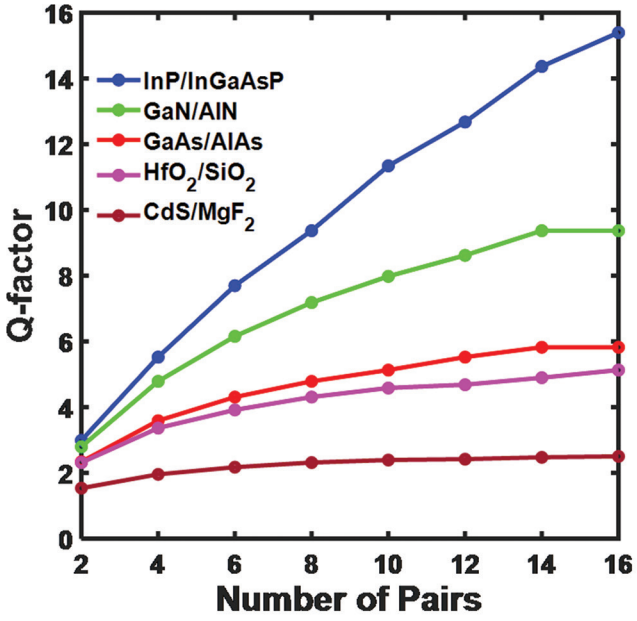

Fig. 10. Q-factor versus number of pairs for various inorganic compounds.

Initially, increasing the number of CdS/MgF_2 layer pairs reduces the FWHM by sharpening the reflectance peaks, which leads to a corresponding increase in the Q-factor. However, beyond around 8–10 pairs, this narrowing effect begins to saturation, and further additions of layer pairs have a diminishing impact on the reflectance bandwidth. This is particularly true for high refractive index contrast systems like CdS/MgF_2, where strong optical interference is already achieved with relatively few pairs. As a result, the Q-factor curve flattens out and reaches a plateau, stabilizing around 2.51 at 16 pairs. This plateau indicates the limit of performance enhancement through additional layering in this DBR configuration.

A lower Q-factor is advantageous in the design of broadband optical structures, including reflectors, antireflection coatings, and light extraction layers such as LEDs, solar cells (Sakoda and Sakoda, 2005), photodetectors, and specific types of optical filters (Macleod and Macleod, 2010).

IV. Conclusion

In this study, a CdS/MgF_2-based DBR was designed and analyzed for operation at 650 nm within the visible spectrum. The TMM simulations confirmed that a high refractive index contrast significantly enhances reflectivity and overall optical performance. Compared to traditional DBR structures, the proposed design achieved superior reflectivity with only 6 pairs, emphasizing its efficiency and practical advantages. The CdS/MgF_2 combination exhibited the broadest usable and theoretical stopband width, the highest FWHM, and a significantly moderate Q-factor. These results confirm that CdS/MgF_2 is not only effective for producing high-performance DBRs with a reduced number of layer pairs but also highly suitable for integration into compact, high-efficiency optical systems. Its outstanding optical properties make it a strong candidate for a wide range of optoelectronic applications, including VCSELs, optical filters, LEDs, and other advanced photonic technologies.

References

Adachi, S., 1989. Optical dispersion relations for GaP, GaAs, GaSb, InP, InAs, InSb, Al x Ga1− x As, and In1− x Ga x As y P1− y. *Journal of Applied Physics*, 66, pp.6030-6040.

Alias, M.S., Alatawi, A.A., Chong, W.K., Tangi, M., Holguin-Lerma, J.A., Stegenburgs, E., Shakfa, M.K., Ng, T.K., Albadri, A.M., and Alyamani, A.Y., 2018. High reflectivity YDH/SiO2 distributed Bragg reflector for UV-C wavelength regime. *IEEE Photonics Journal,* 10, pp.1-8.

AL-Kuhaili, M., 2004. Optical properties of hafnium oxide thin films and their application in energy-efficient windows. *Optical Materials*, 27, pp.383-387.

Aspnes, D., Kelso, S., Logan, R., and Bhat, R., 1986. Optical properties of Al x Ga1− x As. *Journal of Applied Physics*, 60, pp.754-767.

Aspnes, D.E., and Studna, A., 1983. Dielectric functions and optical parameters of si, ge, gap, gaas, gasb, inp, inas, and insb from 1.5 to 6.0 ev. *Physical Review B,* 27, p.985.

Assafli, H.T., Abdulhadi, A.H., and Nassir, W.Y., 2016. Design high efficient reflectivity of distributed bragg reflectors. *Iraqi Journal of Laser*, 15, pp.13-18.

Barker, A. Jr., and Ilegems, M., 1973. Infrared lattice vibrations and free-electron dispersion in GaN. *Physical Review B*, 7, p.743.

Bieniewski, T., and Czyzak, S., 1963. Refractive indexes of single hexagonal ZnS and CdS crystals. *Journal of the Optical Society of America*, 53, pp.496-497.

Butt, M.A., Fomchenkov, S.A., Ullah, A., Habib, M., and Ali, R.Z., 2016. Modelling of multilayer dielectric filters based on TiO2/SiO2 and TiO2/MgF2 for fluorescence microscopy imaging. *Компьютерная Оптика,* 40, pp.674-678.

Byrnes, S.J., 2016. Multilayer Optical Calculations. *arXiv preprint arXiv:1603.02720*.

Chaqmaqchee, F.A., 2016. Optical design of dilute nitride quantum wells vertical cavity semiconductor optical amplifiers for communication systems. *ARO-The Scientific Journal of Koya University,* 4, pp.8-12.

Chaqmaqchee, F.A.I., 2012. *Electrically Pumped GaInNAs Vertical Cavity Semiconductor Optical Amplifiers for Operation at 1.3 [mu] m Wavelength.* University of Essex, England.

Chaqmaqchee, F.A.I., 2022. Temperature stable 980 nm InGaAs/GaAsP vertical cavity surface emitting lasers for short-reach links. *Journal of Optoelectronics and Advanced Materials*, 24, pp.312-317.

Chaqmaqchee, F.A.I., Salh, S.A.A., and Sabri, M.F.M., 2020. Optical analysis of 1300 nm GaInNAsSb/GaAs vertical cavity semiconductor optical amplifier. *Zanco Journal of Pure and Applied Sciences*, 32, pp.87-92.

Coldren, L.A., Corzine, S.W., and Mashanovitch, M.L., 2012. *Diode Lasers and Photonic Integrated Circuits*. John Wiley & Sons, New Jersey.

Cui, M., Guo, C., Yang, Z., Chen, L., Dai, Y., Xu, H., Guo, W., and Ye, J., 2022. Conductive SiO2/HfO2 distributed Bragg reflector achieved by electrical breakdown and its application in GaN-based light emitters. *Journal of Applied Physics*, 131, p.045301.

Dai, J., Gao, W., Liu, B., Cao, X., Tao, T., Xie, Z., Zhao, H., Chen, D., Ping, H., and Zhang, R. 2016. Design and fabrication of UV band-pass filters based on SiO2/Si3N4 dielectric distributed bragg reflectors. *Applied Surface Science,* 364, pp.886-891.

Dodge, M.J., 1984. Refractive properties of magnesium fluoride. *Applied Optics*, 23, pp.1980-1985.

Fern, R., and Onton, A., 1971. Refractive index of AlAs. *Journal of Applied Physics*, 42, pp.3499-3500.

Gao, B., George, J.P., Beeckman, J., and Neyts, K., 2020. Design, fabrication and characterization of a distributed Bragg reflector for reducing the étendue of a wavelength converting system. *Optics Express*, 28, pp.12837-12846.

Haglund, E.P., Kumari, S., Westbergh, P., Gustavsson, J.S., Baets, R.G., Roelkens, G., and Larsson, A., 2016. 20-Gb/s modulation of silicon-integrated short-wavelength hybrid-cavity VCSELs. *IEEE Photonics Technology Letters,* 28, pp.856-859.

Jambunathan, R., and Singh, J., 1997. Design studies for distributed Bragg reflectors for short-cavity edge-emitting lasers. *IEEE Journal of Quantum Electronics,* 33, pp.1180-1189.

Jambunathan, R., and Singh, J., 2002. Design studies for distributed Bragg reflectors for short-cavity edge-emitting lasers. *IEEE Journal of Quantum Electronics,* 33, pp.1180-1189.

Kogelnik, H., and Shank, C.V., 1972. Coupled-wave theory of distributed feedback lasers. *Journal of Applied Physics,* 43, pp.2327-2335.

Kumar, R., Thakor, K., Gupta, S., Maripeddi, R., Nag, D., and Laha, A., 2019. *Design and Optimization of Dielectric DBR for VCSEL, Targeting Emission Range of 520-550nm.* Technical Report. Indian Institute of Technology Bombay.

Ma, G., Shen, J., Zhang, Z., Hua, Z., and Tang, S.H., 2006. Ultrafast all-optical switching in one-dimensional photonic crystal with two defects. *Optics Express,* 14, pp.858-865.

Macleod, H.A., and Macleod, H.A., 2010. *Thin-film Optical Filters*. CRC Press, United States.

Malitson, I.H., 1965. Interspecimen comparison of the refractive index of fused silica. *Journal of the Optical Society of America*, 55, pp.1205-1209.

Miao, W.C., Hong, Y.H., Hsiao, F.H., Chen, J.D., Chiang, H., Lin, C.L., Lin, C.C., Chen, S.C., and Kuo, H.C., 2023. Modified distributed Bragg reflectors for color stability in InGaN red micro-LEDs. *Nanomaterials (Basel)*, 13, p.661.

Min, T., Zhuo-Ying, L., Yao-Lin, H., Jing-Chen, J., and Ye-Hui, P., 2022. Optimal design of thermal emitter based on DBR cavity model in thermal photovoltaic technology. *Results in Optics,* 9**,** p.100322.

Mohammed, Z.H., 2019 The fresnel coefficient of thin film multilayer using transfer matrix method tmm. In: *IOP Conference Series: Materials Science and Engineering*. IOP Publishing, p.032026.

Muallem, M., Palatnik, A., Nessim, G.D., and Tischler, Y.R., 2015. Room temperature fabrication of dielectric bragg reflectors composed of a caf2/zns multilayered coating. *ACS Applied Materials and Interfaces*, 7*,* pp.474-481.

Palo, E., and Daskalakis, K.S., 2023. Prospects in broadening the application of planar solution-based distributed Bragg reflectors. *Advanced Materials Interfaces,* 10, p.2202206.

Pastrňák, J., and Roskovcová, L., 1966. Refraction index measurements on AlN single crystals. *Physica Status Solidi (B),* 14, pp.K5-K8.

Polyanskiy, M.N., 2024. Refractiveindex. info database of optical constants. *Scientific Data,* 11, p.94.

Rodríguez Lamoso, I., and Preu, S., 2025. High reflectivity, compact, and widely tunable distributed bragg reflector based on silicon-rich SiN x-SiO y at 80° C PECVD. *Applied Sciences,* 15, p.3330.

Sakoda, K., and Sakoda, K., 2005. *Optical Properties of Photonic Crystals*. Springer, Berlin.

Sale, T.E., 1995. *Vertical Cavity Surface Emitting Lasers.* Research Studies Press, Wiley, Taunton, Somerset, England, New York.

Sediq, K.N., Muhammadsharif, F.F., and Muhammad, H.A., 2022. A study on tuning the optical properties of stacked SiN/SiO2 mirrors in distributed Bragg's reflectors. *Journal of Optics,* 51, pp.937-942.

Sediq, K.N., Muhammadsharif, F.F., Ramadan, S.O., and Sedeeq, S.Z., 2023. Design and study of a nanocavity-based one-dimensional photonic crystal for potential applications in refractive index sensing. *Aro-The Scientific Journal of Koya University,* 11, pp.95-98.

Shaaban, I.E., Samra, A.S., Muhammad, S., and Wageh, S., 2022. Design of distributed bragg reflectors for green light-emitting devices based on quantum dots as emission layer. *Energies*, 15, p.1237.

Sharhan, A.A., 2020. Transfer matrix mathematical method for evaluation the DBR mirror for light emitting diode and laser. *Journal of Physics: Conference Series*. IOP Publishing, p.012018.

Troitskiĭ, Y.V., 2002. The energy conservation law for optical two-port devices. *Optics and Spectroscopy,* 92, pp.555-559.

Valligatla, S., Chiasera, A., Varas, S., Bazzanella, N., Rao, D.N., Righini, G.C., and Ferrari, M., 2012. High quality factor 1-D Er3+-activated dielectric microcavity fabricated by RF-sputtering. *Optics Express,* 20, pp.21214-21222.

Xu, K., Meng, Y., Chen, S., Li, Y., Wu, Z., and Jin, S., 2021. All-dielectric color filter with ultra-narrowed linewidth. *Micromachines,* 12, p.241.

Yariv, A., 1997. *Optical Electronics in Modern Communications*. Oxford University Press, Oxford.

Yeh, P., and Hendry, M., 1990. *Optical Waves in Layered Media*. American Institute of Physics, United States.

Zhang, C., Elafandy, R., and Han, J., 2019. Distributed Bragg reflectors for GaN-based vertical-cavity surface-emitting lasers. *Applied Sciences,* 9, p.1593.